

MIT Open Access Articles

Characterisation of lightly oxidised organic aerosol formed from the photochemical aging of diesel exhaust particles

The MIT Faculty has made this article openly available. **Please share** how this access benefits you. Your story matters.

Citation: Kroll, Jesse H. et al. "Characterisation of Lightly Oxidised Organic Aerosol Formed from the Photochemical Aging of Diesel Exhaust Particles." Environmental Chemistry 9.3 (2012): 211. Web.

As Published: <http://dx.doi.org/10.1071/EN11162>

Publisher: CSIRO Publishing

Persistent URL: <http://hdl.handle.net/1721.1/72168>

Version: Author's final manuscript: final author's manuscript post peer review, without publisher's formatting or copy editing

Terms of use: Creative Commons Attribution-Noncommercial-Share Alike 3.0



1 **Characterization of lightly oxidized organic aerosol formed from the photochemical aging**
2 **of diesel exhaust particles**

3
4 Jesse H. Kroll^{1,2,*}, Jared D. Smith^{3,†}, Douglas R. Worsnop⁴, and Kevin R. Wilson³

5
6 ¹ *Department of Civil and Environmental Engineering, Massachusetts Institute of Technology,*
7 *Cambridge MA 02139*

8 ² *Department of Chemical Engineering, Massachusetts Institute of Technology, Cambridge MA*
9 *02139*

10 ³ *Chemical Sciences Division, Lawrence Berkeley National Laboratory, Berkeley CA 94720*

11 ⁴ *Center for Aerosol and Cloud Chemistry, Aerodyne Research Inc., Billerica MA 01821*
12

13 *corresponding author; email jhkroll@mit.edu, phone 617-253-2409

14 † *present address: L.J. Smith and Associates, Rogers AR*
15
16

17 **Environmental Context.** The health and climate impacts of atmospheric fine particulate matter
18 (aerosols) may be seriously affected by the chemical transformations that the particles undergo in
19 the atmosphere, but these “aging” reactions are poorly understood. Here we age diesel exhaust
20 particles in the laboratory in order to better understand how they may evolve in the atmosphere,
21 and find subtle but unmistakable changes in their chemical composition. These results provide a
22 more complete picture of the atmospheric evolution of aerosol for inclusion in atmospheric
23 models.
24
25

Abstract. The oxidative aging of the semivolatile fraction of diesel exhaust aerosol is studied in order to better understand the influence of oxidation reactions on particle chemical composition. Exhaust is sampled from an idling diesel truck, sent through a denuder to remove gas-phase species, and oxidized by hydroxyl (OH) radicals in a flow reactor. OH concentrations are chosen to approximately match OH exposures a particle would experience over its atmospheric lifetime. Evolving particle composition is monitored using aerosol mass spectrometry in two different modes, electron impact ionization (EI) for the measurement of elemental ratios, and vacuum ultraviolet (VUV) photoionization for the measurement of molecular components. Changes to mass spectra in both modes indicate major changes to particle composition over the range of OH exposures studied. The product aerosol is only lightly oxidized ($O/C < 0.3$), suggesting an intermediate oxidation state between primary organics and the highly oxidized organic aerosol observed in the atmosphere. These lightly oxidized organics appear to be composed of secondary organic aerosol from semivolatile species, as well as from heterogeneously oxidized particle-phase organics. Key chemical characteristics (elemental ratios, oxidation kinetics, and mass spectrometric features) of the reaction system are examined in detail. Similarities between this laboratory-generated aerosol and “hydrocarbon-like organic aerosol” (HOA) reported in ambient studies suggest that HOA might not be entirely primary in origin, as is commonly assumed, but rather might include a significant secondary component.

Introduction.

Recent work has shown that organic aerosol (OA) generated under standard laboratory conditions tends to be substantially less oxidized than ambient OA [1-5]. This difference strongly suggests that most laboratory studies – and therefore many model treatments – do not capture the full extent of oxidation that organics undergo in the atmosphere. Instead, ongoing oxidation in the atmosphere will result in continual changes to the composition, loading, and properties of OA over its atmospheric lifetime (days to weeks). As a result, there is intense interest in better understanding the chemistry (kinetics, mechanism, and products) of aerosol aging processes [6, 7].

Recent aging studies have focused on the heterogeneous oxidation of organic aerosol particles by the hydroxyl (OH) radical [8-19], in order to better understand the rates and key chemical steps associated with the oxidative degradation of particulate organic compounds. In our previous work on this topic [15-19] we have studied the oxidation of single-component model aerosol systems, simplifying the analysis of the reaction kinetics and products. In these experiments the particles were exposed to very high OH concentrations (up to the equivalent of several weeks in the atmosphere) in order to probe how later-generation (oxidized) products may themselves age in the atmosphere. While this intensive oxidation of single-component particles is useful for understanding key details of aging chemistry, these experimental conditions make it difficult to compare the aged OA in our experiments to that found in the atmosphere.

In this study we utilize our same general experimental approach to examine aerosol aging under more atmospherically relevant conditions. Rather than examine the chemistry of single model compounds, here we oxidize diesel exhaust aerosol, a highly complex mixture of reduced organics. Diesel exhaust includes high concentrations of gas-phase species — volatile organic

compounds (VOCs) and intermediate-volatility organic compounds (IVOCs) — which have been shown to form secondary organic aerosol (SOA) very efficiently upon oxidation [6, 20]. In order to probe the oxidative chemistry of only the lowest-volatility components of the aerosol, we therefore remove these gas-phase species prior to oxidation. Further, these experiments utilize a much more modest range of OH exposures than in our previous studies, allowing us to study only those oxidative transformations that may occur over the atmospheric lifetime of the OA.

Experimental.

The experimental setup used for this study is shown in Figure 1. With the exception of the method used for introducing the aerosol (diesel exhaust), this setup is identical to the one used in our previous experiments of the heterogeneous oxidation of model organic compounds, and is described only briefly here. Experiments were carried out at the Advanced Light Source (ALS) at Lawrence Berkeley National Laboratory, Berkeley CA. Diesel exhaust is sampled directly from the tailpipe of an idling truck (2000 Dodge Ram 3500) located just outside the laboratory. The vehicle, which runs on NA1993 ultra-low sulfur diesel and has no specific emissions control technology, is run in idling mode only; the effect of higher engine loads (which generally involve lower emissions of organics [21]) is not investigated in this study. The sampling inlet (a 3/8" copper tube) is located ~5 cm from the tailpipe. The exhaust is then pulled at 1.3 L/minute into the laboratory via a 3/8" diameter, ~10 m long unheated tube to our experimental setup.

Exhaust is first sent through a 1 m long annular charcoal denuder to remove gas-phase species. (Losses of particles and low-volatility gas-phase organics may occur in the sampling line as well.) A fraction of the flow is sent into a scanning mobility particle sizer (SMPS, TSI

Inc.) to monitor the concentration and size distribution of the sampled particles. Surface-weighted mean diameters of the particles are ~125-145 nm, with particle mass concentrations varying from 400 to 1000 $\mu\text{g}/\text{m}^3$.

The remainder of the diesel exhaust flow is sent into our flow reactor, a quartz flow tube with a length of 130 cm, inner diameter of 2.5 cm, and residence time of ~37 s. Oxidation is initiated by hydroxyl (OH) radicals, generated by the photolysis of ozone in the presence of water. This requires that additional flows be added to the aerosol flow prior to the reactor. These flows include humidified nitrogen (relative humidity of 30%), oxygen, and ozone (generated from a corona discharge ozone generator). Together these flows dilute the aerosol flow by less than 50%. Within the flow tube, ozone is photolyzed by 254 nm light from two mercury lamps positioned just outside the quartz tube; these lamps also heat the tube somewhat, up to a temperature of ~35°C. O_3 photolysis generates $\text{O}(^1\text{D})$, which reacts with water vapor to form hydroxyl radicals (OH). A trace amount of hexane (~100 ppb) is added to the tube, and measured by GC-FID to quantify OH exposure [15]. OH concentrations, controlled by varying $[\text{O}_3]$, range from $\sim 1.1 \times 10^9$ to 8×10^{10} molecule cm^{-3} . The resulting OH exposures correspond to the equivalent of 4 hours to 11 days in the atmosphere, assuming an average ambient OH concentration of 3×10^6 molecules cm^{-3} (though chemistry occurring over such short reaction times probably cannot be so simply extrapolated to atmospheric conditions [14, 17]). Higher levels of OH in the flow tube are possible, and have been accessed in our previous studies, but the focus of this work is on the initial oxidation of the diesel exhaust only. Nitrogen oxides (not measured in this experiment) in the exhaust might modify the subsequent oxidation chemistry somewhat, specifically via the reaction of NO with RO_2 ; however we expect this reaction to be of minor importance due to the suppression of NO by the high concentrations of O_3 and HO_2 .

The composition and size of particles exiting the flow reactor are measured using a high-resolution time-of-flight aerosol mass spectrometer (HR-ToF-AMS, Aerodyne Research, Inc.), as well as a second SMPS (TSI Inc.). The AMS was modified to allow for two modes of ionization of the aerosol components, electron impact ionization (EI, the standard AMS approach), and vacuum ultraviolet photoionization (VUV) [22]. For EI, the vaporizer temperature is set to 600°C, and the mass spectrum (using W-mode) and vacuum aerodynamic diameter (using V-mode) are measured. The high resolution of the mass spectrometer enables the determination of elemental ratios (O/C and H/C), using the approach of Aiken et al. [23, 24]. For VUV mode, radiation from the Chemical Dynamics Beamline (Beamline 9.0.2) of the ALS is used to photoionize the organics within the ionization region of the AMS. The low photon energy used (10.5 eV) minimizes ion fragmentation, allowing for improved identification of aerosol components [25-27]. We note that even when produced by VUV ionization, oxygenated organic ions tend to fragment considerably [15], precluding the molecular identification of the product species. Because of the lower sensitivity associated with photoionization, for VUV measurements the AMS is run in V-mode only, with no particle sizing. For such measurements the vaporizer temperature is set to 100°C, in order to minimize thermal energy imparted to the ions (which also contributes to fragmentation [28]). Thus the diesel oxidation experiments are carried out twice, first with the AMS in EI mode at 600°C and then with the AMS in VUV mode at 100°C. At this lower temperature there is significant aerosol signal in the “closed” mode of the AMS (when the aerosol beam is blocked), suggesting relatively slow vaporization. As a result, all reported VUV mass spectra are from running in “open” mode only (as opposed to the standard “difference” mode).

The combined SMPS/AMS measurements allow particle mass to be determined, by multiplying average particle volume (from the SMPS) by the effective particle density. This is turn is computed from the ratio of vacuum aerodynamic diameter (as measured in by the AMS in particle-time-of-flight mode) to mobility diameter (as measured by the SMPS) [29]. This calculation assumes the particles are spherical, which is not strictly true due to the likely presence of elemental carbon (EC) in the particles [21]. However, since the particles are rich in aliphatic organics they are unlikely to be highly irregular in shape, and so the presence of EC is not expected to introduce significant errors in the particle mass calculation [29].

Results.

Evolving mass spectra. Figure 2 shows normalized unit-mass-resolution (UMR) EI and VUV mass spectra for unreacted diesel exhaust, as well as exhaust exposed to differing levels of OH. With the exception of changes in ozone concentrations (which control OH exposure) and drifts in the sampled particle number concentrations, reaction conditions (flows, irradiation by the mercury lamps, relative humidity, temperature, etc.) are held constant over all experiments. The mass spectra of the particles undergo marked changes with oxidation, indicating that the low-volatility (particulate) fraction of the diesel exhaust is subject to chemical changes over its atmospheric lifetime.

The EI spectra (Fig. 2a-d) are dominated by low-mass ions, due to the high degree of ion fragmentation associated with this ionization technique. Changes in the EI spectra with oxidation involve shifts in the relative intensities of the different ion masses, including (1) the increasing intensity of ions at m/z 44 and 45, (2) the decreasing intensity of higher-mass ions ($m/z > 45$), and (3) shifts in the relative intensities within each ion “cluster” (e.g., m/z 40-45, 53-

59, 65-73, etc.). These first two changes, which are necessarily related, are observed regularly in AMS studies, with m/z 44 being a major indicator of organic acids and related species [30]. At the same time, none of these spectra appear to have reached the high degree of oxidation of “oxidized organic aerosol” (OOA) observed in ambient conditions [7, 24, 31]. This suggests that over these OH exposures, these experiments are accessing an intermediate oxidation state, forming particulate organics that are only lightly oxidized. The third change to the spectra, which involves a shift to lower “delta series” of the ions [1, 32], reflects more subtle shifts in particle composition, and is discussed in a later section.

The VUV mass spectra (Fig. 2e-h) exhibit high ion intensity over a much wider range of masses, as expected for this soft ionization technique. The high-mass mode (right side of each spectrum, m/z 300-500) corresponds mostly to molecular ions, which have masses corresponding to aliphatic hydrocarbons (21-36 carbon atoms per molecule). The most intense peak in the mass spectrum of the unoxidized exhaust aerosol is at 338.39, corresponding to $C_{24}H_{50}$. The lower-mass peaks ($m/z < 300$) are likely to be dominated by fragment ions. When viewed in high-resolution, all major peaks exhibit large positive mass defects (with exact masses substantially above their integer values), indicating high hydrogen content; this confirms the dominance of aliphatic organics in the exhaust. Peaks corresponding to hydrogen-poor polycyclic aromatic hydrocarbons (e.g., $C_{20}H_{12}^+$, m/z 252.09, corresponding to benzo[a]pyrene) are also observed, but these are very small compared to their corresponding aliphatic isobaric ions (e.g., $C_{18}H_{36}^+$, m/z 252.28). Thus polycyclic aromatic hydrocarbons likely represent a minor component of the particles, consistent with results from previous studies [33].

The VUV aerosol mass spectrum changes much more dramatically upon oxidation than does the EI spectrum, with a rapid decrease in the intensity of the high-mass mode (molecular

ions) and a corresponding increase in the lower-mass peaks (fragment ions). This is because oxygen-containing species fragment much more readily upon VUV photoionization than do reduced species; thus as the aerosol becomes more oxidized, the degree of ion fragmentation increases, leading to the large observed shifts in the VUV mass spectra.

Changes in elemental composition of the organics. The high resolution of the EI mass spectra enables the determination of elemental ratios of the particulate organics [23, 24], most importantly the hydrogen-to-carbon ratio (H/C) and the oxygen-to-carbon ratio (O/C). Figure 3a shows the evolving elemental ratios of the organic particulate matter in a “van Krevelen plot”, a plot of H/C vs. O/C. As has been seen in other aliphatic systems [4], the unoxidized (primary) particles begin in the top left of the plot (H/C= 2.06, O/C = 0.025), and move down and to the right upon oxidation. However, even at the highest levels of oxidation accessed in these experiments, the particles are not as oxidized as most ambient OOA fractions [4, 34], again suggesting the resulting particles are in their early stages of oxidation.

Two distinct slopes in Krevelen space are seen. At low levels of oxidation ($O/C < 0.1$), the data follow a slope of -1.93; this is close to the -2 slope associated with the introduction of carbonyl (ketone or aldehyde) functional groups to the condensed-phase organics, suggesting the importance of those moieties in these early stages of oxidation. At higher levels of oxidation, the data instead follow a shallower slope of -0.93, close to the slope of -1 associated with addition of carboxylic acid or hydroxycarbonyl functionalities. This shift in the van Krevelen slope, and therefore in the formation of particle-phase products, is very similar to what we observed in our previous study of the heterogeneous oxidation of squalane [4, 16]. We note that these changes in the elemental ratios result solely from oxidative aging of the aerosol; therefore observations of

similar slopes under ambient conditions may reflect aging chemistry and cannot necessarily be attributed solely to physical (e.g., mixing) processes [4, 34]. Results from other laboratory and field studies show that at even higher levels of oxidation, the slope appears to level off still further, to values of -0.5 [4, 34], reflecting yet another shift in the aging chemistry for more highly oxidized species.

We have previously demonstrated the utility of examining aging chemistry using not only elemental ratios (O/C and H/C) but also elemental abundances (the amount of carbon, hydrogen, and oxygen in the particle phase). In our earlier study of the heterogeneous oxidation of squalane [16], the calculation of elemental abundances allowed for the determination of the relative importance of two key oxidation channels, functionalization (the addition of oxygen-containing functional groups to a carbon skeleton) and fragmentation (the breaking of the carbon skeleton) [16]. Here we calculate elemental abundances of the diesel exhaust particles from particle mass and elemental ratios, using the same approach as in that study [16]. To account for possible changes in the amount of exhaust sampled into the tube, elemental abundances are corrected for changes to particle number concentration, as measured by the first SMPS (located upstream of the flow reactor).

Figure 3b shows the elemental abundances of carbon and oxygen as functions of OH exposure. As expected, oxygen content increases at higher levels of OH. Additionally, carbon content also increases; this is in marked contrast to the heterogeneous oxidation of squalane [16] (as well as of other model organic species [18]), which exhibits decreases in carbon content due to fragmentation reactions. This new particulate carbon provides strong evidence for the formation of secondary organic aerosol (SOA), from the oxidation of gas-phase organics followed by gas-to-particle conversion. Indeed, at all but the lowest OH exposures, the SMPS

detects a nucleation mode; this new mode contributes negligibly to particle mass but provides unambiguous evidence for SOA formation. At higher OH exposures (not shown), the increased mass from SOA drops rather abruptly, though does not disappear entirely; it is unclear whether this drop is related to a change in the engine output or is a real chemical effect. In any case, the charcoal denuder between the sample inlet and the flow reactor, intended to scavenge all gas-phase SOA precursors, clearly does not prevent the presence of gas-phase organics in the flow tube. This may be due to evaporation of semivolatile material downstream of the denuder, possibly promoted by heating of the flow reactor by the mercury lamps.

Changes in relative ion intensities in EI. As shown in Figure 2, the relative intensities of ions of different nominal masses within each “cluster” of the EI spectra change upon oxidation, with increased oxidation leading to decreases in higher-mass ions and increases in the lower-mass ions. This evolution can be described in terms of the ion (or “delta”) series approach, which classifies organics in an EI mass spectrum by grouping ions that differ by 14 mass units (corresponding to the addition or subtraction of CH_2) [1, 32]. In this approach, each series is assigned a “delta value” (Δ) equal to $m/z - 14n + 1$, where n is an integer nominally equal to the number of CH_2 groups in the ion. In the system studied here, the mass spectrum of unoxidized diesel exhaust particles (Figure 2a) is dominated by the $\Delta = +2$ series, which consists of ions at m/z 29, 43, 57, 71, etc. As OH levels increase, these $\Delta = +2$ ions give way to ions in the $\Delta = 0$ series (m/z 41, 55, 69...) and the $\Delta = -2$ series (m/z 39, 53, 67...). Such changes are examined in more detail in Figures 4 and 5.

Figure 4 shows changes to the fractional contribution of m/z 43, as well as its delta series ($\Delta = +2$), to total EI signal. At unit mass resolution, the m/z 43 fraction (heavy black curve) is

approximately constant with OH exposure (at ~13% of total ion signal). However, examination of the high-resolution mass spectrum shows that the two ions that dominate the signal at this nominal mass, C_3H_7^+ (m/z 43.055) and $\text{C}_2\text{H}_3\text{O}^+$ (m/z 43.018), change dramatically over this range of OH exposures. The C_3H_7^+ ion, which accounts for virtually all the m/z 43 signal in the unoxidized particles, quickly drops with OH exposure (solid red curve), whereas the $\text{C}_2\text{H}_3\text{O}^+$ (solid blue curve) grows in; these changes approximately cancel each other out, leading to the constant m/z 43 fraction. The entire $\Delta=+2$ series (m/z 43, 57, 71, 85...), shown as dotted curves in Figure 4, behaves similarly, with a decrease in the $\text{C}_x\text{H}_{2x+1}^+$ fraction counterbalanced by an increase in the $\text{C}_y\text{H}_{2y-1}\text{O}^+$ fraction. However, for the larger mass ions, the two changes do not completely cancel, leading to an overall decrease in the fractional intensity of the $\Delta=+2$ series as a whole. These results point to the importance of isobaric ions (which differ in the number of oxygen atoms) in the oxidative evolution of organic particles, and highlight the utility of high-resolution MS for understanding the mechanisms of aerosol aging.

However, this shift to more oxygenated ions does not explain all the changes in the relative ion intensities seen in the EI spectra. Shown in Figure 5 are the evolving fractional contributions of each C_xH_y^+ delta series to the total C_xH_y^+ signal. Even though all the species included are nominally hydrocarbon ions, their relative intensities vary dramatically with oxidation. The hydrocarbon ions in the $\Delta=+2$ series ($\text{C}_x\text{H}_{2x+1}^+$ ions: C_2H_5^+ , C_3H_7^+ , C_4H_9^+ ...) are the major ions in unoxidized diesel exhaust, accounting for almost half the total ion signal. However, this fraction drops rapidly with oxidation, in favor of the lower delta series. After only minimal oxidation, the $\Delta=0$ hydrocarbon ions ($\text{C}_x\text{H}_{2x-1}^+$ ions: C_2H_3^+ , C_3H_5^+ , C_4H_7^+ ...) emerge as the major contributors to C_xH_y^+ signal; however, upon further oxidation even these ions become less dominant, as still lower delta series ($\Delta=-2$, -4 , and -6) increase in importance

throughout. (The odd-numbered delta series, corresponding to the even-mass ions, tend to be minor and do not exhibit any significant trend.) These lower- Δ ions are generally associated with unsaturated hydrocarbons such as alkenes and cycloalkanes [32]; however it seems unlikely the relative abundances of such molecules would increase with OH exposure. Instead we believe these ions are formed from oxygenates, as a result of oxygen loss either on the vaporizer (via thermal/pyrolytic decomposition) or in the ionization region (via neutral loss) in the AMS. Such processes will likely lead to the formation of unsaturated (low- Δ) ions, as is observed. Indeed, the lower hydrogen number of the lower- Δ ions indicates a higher carbon oxidation state [5], and thus it is expected that such ions will increase in abundance at higher OH exposures.

Kinetics and products of oxidative aging. An accurate picture of aerosol aging requires an understanding of the rate of the aging reactions as well as the key chemical properties of the aging products. In our previous studies of the oxidation of single-component model organic particles, it was relatively straightforward to estimate such quantities, by tracking the concentration of the reactant species (usually using a single marker ion in the mass spectrum), and measuring the aerosol composition after depletion of the reactant species [15, 18]. This approach cannot be used for the present studies, since diesel exhaust aerosol involves (at least) hundreds of individual species, precluding the use of individual marker ions.

Instead we utilize a spectral subtraction approach, similar to that used by Sage et al. [35], in which the unreacted diesel exhaust mass spectrum is scaled and subtracted from the mass spectrum of the oxidized aerosol. The largest scaling factor for which no peaks go negative gives an upper limit to the fraction of unreacted organics still present in the particle. All spectra used were normalized to total ion signal; because particle mass increases due to SOA

condensation, this normalization may lead to an oversubtraction, and hence an underestimate (by up to a factor of ~ 2) of the fraction of unreacted organics remaining. This spectral subtraction approach was applied to both the high-resolution EI spectra (m/z 12-120) and the unit-mass-resolution VUV spectra (m/z 40-600). Results (fraction of unreacted diesel exhaust remaining vs. OH exposure) are shown in Figure 6. The fractional loss of the unreacted organics is substantial, exceeding 90% at the highest OH exposures studied. Since this fractional decrease is much larger than the fractional increase of particle mass by SOA condensation (Figure 3b), the unreacted organics are being lost in an absolute sense, rather than simply being diluted by the additional SOA mass. This indicates that the initial aerosol components themselves are undergoing oxidation, which (along with SOA formation) will affect the chemical composition of the particles. Some of this oxidation may occur in the gas phase, via evaporation/oxidation/recondensation of semivolatile species (the “semivolatile pumping” mechanism [36]). However, the residence time in the flow reactor (37 s) may be too short to allow for full semivolatile equilibrium partitioning; thus, the heterogeneous oxidation of particulate organics by gas-phase OH is also likely to play a role in this degradation chemistry.

At low OH exposures ($\leq 3.1 \times 10^{11}$ molecule cm^{-3} s), the unreacted diesel exhaust decays exponentially, with a decay constant (determined from fitting the EI spectral subtraction results in this range) of 3.56×10^{-12} $\text{cm}^3 \text{ molec}^{-1} \text{ s}^{-1}$. (Only one VUV experiment was made in this OH exposure range, and is reasonably consistent with the EI results.) This decay constant corresponds to the second-order rate constant of the OH-particle reaction (k_{OH}), and allows for the determination of the effective uptake coefficient (γ_{OH}), the ratio of the rate of reactive loss of the particulate organics to the OH collision rate with the particle surface [15]. The uptake coefficient is calculated from the rate using the expression

$$\gamma_{\text{OH}} = \frac{2D_0\rho N_A}{3\bar{c}_{\text{OH}}M} k_{\text{OH}} \quad (1)$$

where D_0 is the surface-area-weighted mean particle diameter, ρ is the particle density, M is the average molecular weight of the particle (taken to be 338 g/mol, from Figure 2e), N_A is Avogadro's number, and \bar{c}_{OH} is the mean speed of the hydroxyl radical. The uptake coefficient is calculated to be 0.9; this is higher than our measured values for squalane, but again is likely to be an upper limit, given the spectral subtraction approach used. Due to unknown amounts of secondary chain chemistry and uncertainty with regard to the "semivolatile pumping" mechanism, this uptake coefficient is not explicitly corrected for gas-phase diffusion of OH [37]. Regardless, this value of γ_{OH} is substantially lower than those determined by Lambe et al. for individual semivolatile components within fuel or motor oil [38]. That study was carried out using an environmental chamber, and the high values of γ_{OH} (often well above unity) were taken as evidence of evaporation followed by gas-phase oxidation. The much lower γ_{OH} value determined in our study suggests that such a mechanism does not occur efficiently in our system. This may be a result of the prior removal of the most volatile components of the aerosol by the denuder, the high aerosol loadings used, and/or the short timescales within our flow reactor, any of which could minimize the evaporation of semivolatile species.

At higher OH exposure levels, the decrease in the fraction of unreacted organics appears to slow down, as evidenced by the shallower slopes on the right side of Figure 6. The reason for this apparent slowing of the chemistry is not clear. This shift occurs at roughly the same OH exposure as the change in the slope of the van Krevelen plot (Figure 3a), suggesting it may be related to changes to the oxidation mechanism, but this is only speculative. It should also be noted that the EI and VUV spectral subtraction results diverge considerably at these high OH exposures. This may arise from the difference in selectivity of the two techniques. If the

product spectra share many features with reactant spectra, then this spectral subtraction approach will overestimate the degree to which the reactant is lost. This effect will be most pronounced for the least selective techniques; since EI is relatively unselective, the inferred loss of unreacted organics is expected to be greater for EI than for VUV, as is observed here.

Shown in Figure 7 are residual spectra, obtained by subtracting the mass spectrum of unreacted diesel exhaust (shown at top) from that of the oxidized aerosol at the lowest level of OH exposure studied (4.3×10^{10} molecule cm^{-3} s for EI and 1.7×10^{11} molecule cm^{-3} s for VUV). These spectra represent early-generation oxidation products. For EI, the shifts in the ion intensities towards lower m/z series are evident, and the elemental ratios associated with the residual aerosol ($\text{O/C} = 0.15$, $\text{H/C} = 1.86$) indicate the organics are mildly oxidized. In VUV the residual (product) spectrum exhibits a clear shift towards higher mass peaks, with the most intense ion at m/z 364 (up from m/z 338 for the unreacted diesel exhaust). This may indicate that the lighter molecules react away more rapidly than the heavier ones do. Interestingly, none of the molecular ions in the VUV residual spectrum appear to include oxygen atoms, in stark contrast with our results from heterogeneously oxidized squalane [15]. This suggests that the multiphase oxidation chemistry of diesel exhaust aerosol is fundamentally different than that in our previous studies; further study is required to determine whether this arises from differences in particle volatility, or from something more specific to the chemical components of diesel exhaust aerosol.

Discussion.

In this work we have examined the oxidative aging of diesel exhaust particles, with a focus on (1) the chemistry of the lowest-volatility fraction of the organic aerosol (particulate organics and

gas-phase semivolatiles) and (2) the initial stages of oxidation, before the formation of highly oxidized species. The evolution of the elemental ratios of the particulate organics (Figure 3a) is found to be similar to that of the heterogeneous oxidation of squalane [4, 16]. However, from the elemental abundances (Figure 3b) it is clear that the aging pathway for diesel exhaust particles is quite different, involving major contributions by gas-phase oxidation (SOA formation). This underscores the utility of elemental abundances (and not just elemental ratios) for elucidating key processes in aerosol aging. Moreover, it suggests that disparate aging processes may result in products with similar elemental ratios – and hence properties [7, 39] – which may help simplify the modeling of aerosol aging considerably [4].

The aerosol formed in these experiments is only lightly oxidized, with an O/C (and carbon oxidation state) significantly lower than that of the “oxidized organic aerosol” (OOA) component of ambient aerosol. This is apparent in the EI spectra (Fig 2a-d), which lack the intense signal at m/z 44 (CO_2^+) that characterizes OOA. Thus this study confirms previous work (e.g., refs. [13, 40]) indicating that heterogeneous chemistry is too slow to contribute to OOA formation; it also suggests that SOA from low-volatility SVOCs probably cannot form OOA either. In fact the product spectra look similar to those of the “hydrocarbon-like organic aerosol” (HOA) fractions of ambient aerosol, generally taken to be indicative of primary emissions. However, the EI spectra of the lightly oxidized particles (Fig. 2b-d) have some features that distinguish them from the pure primary OA (unreacted diesel exhaust particles, Fig. 2a), such as elevated intensities of oxygen-containing ions and shifts towards ions with fewer hydrogen atoms (lower Δ -series). The dramatic changes to the VUV mass spectra (Fig. 2e-h) provide further evidence of the substantial transformation that the aerosol components undergo as a result of oxidation.

The reaction conditions within our flow reactor (e.g., high oxidant concentrations, high particle loadings, low reaction times, and irradiation at 254 nm) vary considerably from those of the atmosphere. Nonetheless there are some intriguing similarities between the EI spectra of the lightly oxidized aerosol generated in these studies and AMS spectra of ambient aerosol. Ambient HOA spectra tend to have elevated ion intensities at lower delta-series ($\Delta=0, -2$) [41], as well as higher O/C ratios (as high as 0.16) [24, 42, 43], relative to pure hydrocarbon mixtures (such as fuel and lubricating oil). While these spectral features may result from primary OA that includes some oxygen (from sources such as trash-burning [44] or vehicles without aftertreatment devices [20]), they may also indicate early oxidative processing of the primary aerosol. Similarly, AMS measurements just downwind of the 2010 Gulf oil spill [45] found that the OA was relatively unoxidized, with O/C as low as 0.3, particularly in areas most influenced by IVOC (as opposed to VOC) emissions. Such aerosol (which is very likely to be secondary in nature [46]) provides strong evidence for the atmospheric formation of photochemically-generated, lightly-oxidized OA, similar to the aerosol generated in our flow reactor.

The present experiments indicate that low-volatility organic species, in the particle or gas phase, may oxidize to form mildly oxidized organic aerosol over relatively short atmospheric timescales (hours to days). Using the AMS, this aerosol looks quite similar to HOA, generally taken to be purely primary in nature; however the constituent organics may actually be formed from atmospheric oxidation reactions. Thus much of the HOA reported in ambient studies may include a significant secondary (albeit lightly oxidized) component. The resulting aerosol will likely have somewhat different properties than pure primary organic aerosol, which may imply different effects on human health and climate. Future study of the composition, properties, and

chemical signatures of such lightly oxidized organics will help clarify the atmospheric importance and effects of this class of organic particulate matter.

Acknowledgements.

This work was supported by the Director, Office of Energy Research, Office of Basic Energy Sciences, Chemical Sciences Division of the U.S. Department of Energy under Contract No. DE-AC02-05CH11231. J.D.S. was supported by the Camille and Henry Dreyfus Foundation postdoctoral program in environmental chemistry.

References Cited.

1. R. Bahreini, M. D. Keywood, N. L. Ng, V. Varutbangkul, S. Gao, R. C. Flagan, et al., Measurements of secondary organic aerosol from oxidation of cycloalkenes, terpenes, and *m*-xylene using an Aerodyne aerosol mass spectrometer. *Environmental Science and Technology* **2005**, *39*, 5674.
2. P. S. Chhabra, R. C. Flagan, J. H. Seinfeld, Elemental analysis of chamber organic aerosol using an aerodyne high-resolution aerosol mass spectrometer. *Atmos Chem Phys* **2010**, *10*, 4111.
3. P. S. Chhabra, N. L. Ng, M. R. Canagaratna, A. L. Corrigan, L. M. Russell, D. R. Worsnop, et al., Elemental composition and oxidation of chamber organic aerosol. *Atmos Chem Phys* **2011**, *11*, 8827.
4. C. L. Heald, J. H. Kroll, J. L. Jimenez, K. S. Docherty, P. F. DeCarlo, A. C. Aiken, et al., A simplified description of the evolution of organic aerosol composition in the atmosphere. *Geophysical Research Letters* **2010**, *37*, L08803.
5. J. H. Kroll, N. M. Donahue, J. L. Jimenez, S. H. Kessler, M. R. Canagaratna, K. R. Wilson, et al., Carbon oxidation state as a metric for describing the chemistry of atmospheric organic aerosol. *Nature Chemistry* **2011**, *3*, 133.
6. A. L. Robinson, N. M. Donahue, M. K. Shrivastava, E. A. Weitkamp, A. M. Sage, A. P. Grieshop, et al., Rethinking organic aerosols: Semivolatile emissions and photochemical aging. *Science* **2007**, *315*, 1259.
7. J. L. Jimenez, M. R. Canagaratna, N. M. Donahue, A. S. H. Prevot, Q. Zhang, J. H. Kroll, et al., Evolution of Organic Aerosols in the Atmosphere. *Science* **2009**, *326*, 1525.
8. A. T. Lambe, J. Zhang, A. M. Sage, N. M. Donahue, Controlled OH Radical Production via Ozone-Alkene Reactions for Use in Aerosol Aging Studies. *Environmental Science and Technology* **2007**, *41*, 2357.
9. I. L. George, A. Vlasenko, J. G. Slowik, K. Broekhuizen, J. P. D. Abbatt, Heterogeneous oxidation of saturated organic aerosols by hydroxyl radicals: uptake kinetics, condensed-phase products, and particle size change. *Atmospheric Chemistry and Physics* **2007**, *7*, 4187.
10. V. F. McNeill, R. L. N. Yatawelli, J. A. Thornton, C. B. Stipe, O. Landgrebe, Heterogeneous OH oxidation of palmitic acid in single component and internally mixed aerosol particles: vaporization and the role of particle phase. *Atmospheric Chemistry and Physics* **2008**, *8*, 5465.
11. I. J. George, J. Slowik, J. P. D. Abbatt, Chemical aging of ambient organic aerosol from heterogeneous reaction with hydroxyl radicals. *Geophysical Research Letters* **2008**, *35*.
12. I. J. George, J. P. D. Abbatt, Chemical evolution of secondary organic aerosol from OH-initiated heterogeneous oxidation. *Atmospheric Chemistry and Physics* **2010**, *10*, 5551.
13. I. J. George, J. P. D. Abbatt, Heterogeneous oxidation of atmospheric aerosol particles by gas-phase radicals. *Nature Chemistry* **2010**, *2*, 713.
14. L. H. Renbaum, G. D. Smith, Artifacts in measuring aerosol uptake kinetics: the roles of time, concentration and adsorption. *Atmospheric Chemistry and Physics* **2011**, *11*, 6881.
15. J. D. Smith, J. H. Kroll, C. D. Cappa, D. L. Che, C. L. Liu, M. Ahmed, et al., The heterogeneous reaction of hydroxyl radicals with sub-micron squalane particles: a model system for understanding the oxidative aging of ambient aerosols. *Atmospheric Chemistry and Physics* **2009**, *9*, 3209.

16. J. H. Kroll, J. D. Smith, D. L. Che, S. H. Kessler, D. R. Worsnop, K. R. Wilson, Measurement of fragmentation and functionalization pathways in the heterogeneous oxidation of oxidized organic aerosol. *Phys Chem Chem Phys* **2009**, *11*, 8005.
17. D. L. Che, J. D. Smith, S. R. Leone, M. Ahmed, K. R. Wilson, Quantifying the reactive uptake of OH by organic aerosols in a continuous flow stirred tank reactor. *Physical Chemistry Chemical Physics* **2009**, *11*, 7885.
18. S. H. Kessler, J. D. Smith, D. L. Che, D. R. Worsnop, K. R. Wilson, J. H. Kroll, Chemical Sinks of Organic Aerosol: Kinetics and Products of the Heterogeneous Oxidation of Erythritol and Levoglucosan. *Environmental Science & Technology* **2010**, *44*, 7005.
19. S. H. Kessler, T. Nah, K. E. Daumit, J. D. Smith, S. R. Leone, C. E. Kolb, et al., OH-initiated heterogeneous aging of highly oxidized organic aerosol. *J Phys Chem A* **2011**, *in revision*.
20. R. Chirico, P. F. DeCarlo, M. F. Heringa, T. Tritscher, R. Richter, A. S. H. Prevot, et al., Impact of aftertreatment devices on primary emissions and secondary organic aerosol formation potential from in-use diesel vehicles: results from smog chamber experiments. *Atmospheric Chemistry and Physics* **2010**, *10*, 11545.
21. S. D. Shah, D. R. Cocker, J. W. Miller, J. M. Norbeck, Emission rates of particulate matter and elemental and organic carbon from in-use diesel engines. *Environmental Science & Technology* **2004**, *38*, 2544.
22. M. J. Northway, J. T. Jayne, D. W. Toohey, M. R. Canagaratna, A. Trimborn, K. I. Akiyama, et al., Demonstration of a VUV lamp photoionization source for improved organic speciation in an aerosol mass spectrometer. *Aerosol Science and Technology* **2007**, *41*, 828.
23. A. C. Aiken, P. F. DeCarlo, J. L. Jimenez, Elemental Analysis of Organic Species with Electron Ionization High-Resolution Mass Spectrometry. *Analytical Chemistry* **2007**, *79*, 8350.
24. A. C. Aiken, P. F. Decarlo, J. H. Kroll, D. R. Worsnop, J. A. Huffman, K. S. Docherty, et al., O/C and OM/OC ratios of primary, secondary, and ambient organic aerosols with high-resolution time-of-flight aerosol mass spectrometry. *Environ Sci Technol* **2008**, *42*, 4478.
25. E. R. Mysak, K. R. Wilson, M. Jimenez-Cruz, M. Ahmed, T. Baer, Synchrotron radiation based aerosol time-of-flight mass spectrometry for organic constituents. *Analytical Chemistry* **2005**, *77*, 5953.
26. E. Gloaguen, E. R. Mysak, S. R. Leone, M. Ahmed, K. R. Wilson, Investigating the chemical composition of mixed organic-inorganic particles by "soft" vacuum ultraviolet photoionization: The reaction of ozone with anthracene on sodium chloride particles. *International Journal of Mass Spectrometry* **2006**, *258*, 74.
27. S. R. Leone, M. Ahmed, K. R. Wilson, Chemical dynamics, molecular energetics, and kinetics at the synchrotron. *Physical Chemistry Chemical Physics* **2010**, *12*, 6564.
28. K. R. Wilson, M. Jimenez-Cruz, C. Nicolas, L. Belau, S. R. Leone, M. Ahmed, Thermal Vaporization of Biological Nanoparticles: Fragment-Free Vacuum Ultraviolet Photoionization Mass Spectra of Tryptophan, Phenylalanine–Glycine–Glycine, and β -Carotene. *J Phys Chem A* **2006**, *110*, 2106.
29. P. DeCarlo, J. G. Slowik, D. R. Worsnop, P. Davidovits, J. L. Jiménez, Particle Morphology and Density Characterization by Combined Mobility and Aerodynamic Diameter Measurements. Part 1: Theory. *Aerosol Science and Technology* **2004**, *38*, 1185.
30. J. Duplissy, P. F. DeCarlo, J. Dommen, M. R. Alfarra, A. Metzger, I. Barmapadimos, et al., Relating hygroscopicity and composition of organic aerosol particulate matter. *Atmospheric Chemistry and Physics* **2011**, *11*, 1155.

31. Q. Zhang, M. R. Alfara, D. R. Worsnop, J. D. Allan, H. Coe, M. R. Canagaratna, et al., Deconvolution and quantification of hydrocarbon-like and oxygenated organic aerosols based on aerosol mass spectrometry. *Environmental Science and Technology* **2005**, 39, 4938.
32. F. W. McLafferty, F. Turecek. Interpretation of mass spectra. Fourth edition ed. Mill Valley, CA: University Science Books; 1994.
33. J. J. Schauer, M. J. Kleeman, G. R. Cass, B. R. Simoneit, Measurement of Emissions from Air Pollution Sources. 2. C1 through C30 Organic Compounds from Medium Duty Diesel Trucks. *Environ Sci Technol* **1999**, 33, 1578.
34. N. L. Ng, M. R. Canagaratna, J. L. Jimenez, P. S. Chhabra, J. H. Seinfeld, D. R. Worsnop, Changes in organic aerosol composition with aging inferred from aerosol mass spectra. *Atmos Chem Phys* **2011**, 11, 6465.
35. A. M. Sage, E. A. Weitkamp, A. L. Robinson, N. M. Donahue, Evolving mass spectra of the oxidized component of organic aerosol: results from aerosol mass spectrometer analyses of aged diesel emissions. *Atmospheric Chemistry and Physics Discussions* **2007**, 7, 10065.
36. M. A. Miracolo, A. A. Presto, A. T. Lambe, C. J. Hennigan, N. M. Donahue, J. H. Kroll, et al., Photo-Oxidation of Low-Volatility Organics Found in Motor Vehicle Emissions: Production and Chemical Evolution of Organic Aerosol Mass. *Environ Sci Technol* **2010**, 44, 1638.
37. N. Fuchs, A. Sutugin. Highly Dispersed Aerosols. Newton, MA: Butterworth-Heinemann; 1970.
38. A. T. Lambe, M. A. Miracolo, C. J. Hennigan, A. L. Robinson, N. M. Donahue, Effective Rate Constants and Uptake Coefficients for the Reactions of Organic Molecular Markers (n-Alkanes, Hopanes, and Steranes) in Motor Oil and Diesel Primary Organic Aerosols with Hydroxyl Radicals. *Environmental Science & Technology* **2009**, 43, 8794.
39. C. D. Cappa, D. L. Che, S. H. Kessler, J. H. Kroll, K. R. Wilson, Variations in organic aerosol optical and hygroscopic properties upon heterogeneous OH oxidation. *J Geophys Res - Atmos*, **2011**, 116, doi:10.1029/2011JD015918.
40. P. F. DeCarlo, E. J. Dunlea, J. R. Kimmel, A. C. Aiken, D. Sueper, J. Crounse, et al., Fast airborne aerosol size and chemistry measurements above Mexico City and Central Mexico during the MILAGRO campaign. *Atmos Chem Phys* **2008**, 8, 4027.
41. Q. Zhang, D. R. Worsnop, M. R. Canagaratna, J. L. Jimenez, Hydrocarbon-like and oxygenated organic aerosols in Pittsburgh: insights into sources and processes of organic aerosols. *Atmospheric Chemistry and Physics* **2005**, 5, 3289.
42. A. C. Aiken, D. Salcedo, M. J. Cubison, J. A. Huffman, P. F. DeCarlo, I. M. Ulbrich, et al., Mexico City aerosol analysis during MILAGRO using high resolution aerosol mass spectrometry at the urban supersite (T0) - Part 1: Fine particle composition and organic source apportionment. *Atmospheric Chemistry and Physics* **2009**, 9, 6633.
43. P. F. DeCarlo, I. M. Ulbrich, J. Crounse, B. de Foy, E. J. Dunlea, A. C. Aiken, et al., Investigation of the sources and processing of organic aerosol over the Central Mexican Plateau from aircraft measurements during MILAGRO. *Atmospheric Chemistry and Physics* **2010**, 10, 5257.
44. C. Mohr, J. A. Huffman, M. J. Cubison, A. C. Aiken, K. S. Docherty, J. R. Kimmel, et al., Characterization of Primary Organic Aerosol Emissions from Meat Cooking, Trash Burning, and Motor Vehicles with High-Resolution Aerosol Mass Spectrometry and Comparison with Ambient and Chamber Observations. *Environmental Science & Technology* **2009**, 43, 2443.

- 558 45. R. Bahreini, S. A. McKeen, A. M. Middlebrook, K. E. Daumit, A. T. Lambe, M. R.
559 Canagaratna, et al., Characteristics of organic aerosols formed downwind of the Deepwater
560 Horizon site after its explosion. *Environmental Science & Technology* **2011**, *in preparation*.
561 46. J. A. de Gouw, A. M. Middlebrook, C. Warneke, R. Ahmadov, E. L. Atlas, R. Bahreini, et
562 al., Organic Aerosol Formation Downwind from the Deepwater Horizon Oil Spill. *Science*
563 **2011**, *331*, 1295.
564
565
566

Figure captions.

Figure 1. The experimental setup (sample line, flow reactor, and analytical instrumentation) used in this work. See text for details.

Figure 2. Mass spectra (shown in unit-mass resolution) of diesel exhaust particles at different levels of oxidation. The top panels (a and e) correspond to unreacted diesel exhaust; lower panels correspond to particles after exposure to different OH levels (OH exposures are provided in each panel, in units of molecules cm^{-3} s). Left panels (a-d): electron impact ionization (EI) mass spectra. Right panels (e-h): vacuum ultraviolet photoionization (VUV) mass spectra. The peak at m/z 281 corresponds to a siloxane impurity, as confirmed by high-resolution analysis.

Figure 3. Evolving elemental composition of the diesel exhaust particles. Panel a: van Krevelen plot, with oxidation involving movement down and to the right. The trajectories follow two slopes, first -1.93 then -0.93. Both linear fits (determined from the six least-oxidized and the seven most-oxidized systems, respectively) are shown. Panel b: abundances of particulate carbon (green) and oxygen (blue) in the particles, normalized to the amount of carbon in the unreacted system, as a function of OH exposure [16]. The increase in carbon abundance indicates the formation of secondary organic aerosol, presumably from gas-phase semivolatile organics.

Figure 4. Normalized EI signal (ion intensity as a fraction of total) of the m/z 43 ions (solid lines) and all ions in the $\Delta=+2$ series (dotted lines). Changes to individual ions, as determined at high resolution, are much more dramatic than at a given nominal mass, due to the simultaneous decrease in $\text{C}_x\text{H}_{2x+1}^+$ ions and increase in $\text{C}_y\text{H}_{2y-1}\text{O}^+$ ions.

Figure 5. Evolution of the hydrocarbon ions (of form C_xH_y^+) in the EI mass spectra. Contributions of C_xH_y^+ ions in each delta series, as a fraction of the total C_xH_y^+ signal, are plotted against OH exposure. As oxidation increases, the $\Delta=+2$ series gives way to $\Delta=0$, as well as to $\Delta=-2$, -4 , and -6 . These lower Δ -series hydrocarbon ions are likely derived from oxidized organics, which may lose oxygen during heating or ionization within the AMS.

Figure 6. Reactive loss of the particulate organics in diesel exhaust. The fraction of unreacted organics remaining in the particle, as calculated by spectral subtraction (see text), is plotted versus OH exposure, for both EI and VUV data. The solid line is an exponential fit to the initial decay (EI data only), allowing for the determination of the reaction rate and effective uptake coefficient.

Figure 7. Reactant and product mass spectra for the initial aging of diesel exhaust particles. Top panels: unreacted diesel exhaust particles in EI and VUV (same as Fig. 2a and 2e, respectively). The EI spectra are colored by the mass contribution of different elements at each nominal m/z value. Bottom panels: EI and VUV product mass spectra, determined from spectral subtraction of the unreacted spectra from the spectra of oxidized diesel exhaust particles, at the lowest level of OH exposure studied (4.3×10^{10} molecule cm^{-3} s for EI and 1.7×10^{11} molecule cm^{-3} s for VUV). Vertical dashed lines highlight key differences in the residual spectra: major $\Delta=+2$

612 masses (m/z 57, 71, and 85) for EI, and the most intense molecular peaks (m/z 338 and 364) for
613 VUV.
614

Figures.

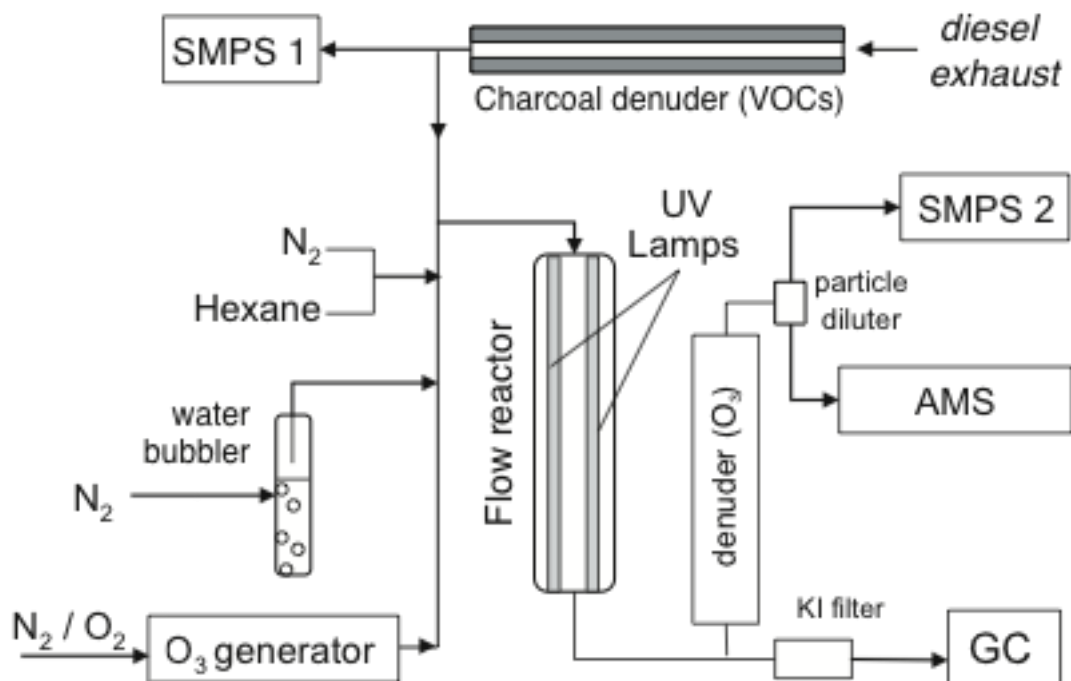


Figure 1. The experimental setup (sample line, flow reactor, and analytical instrumentation) used in this work. See text for details.

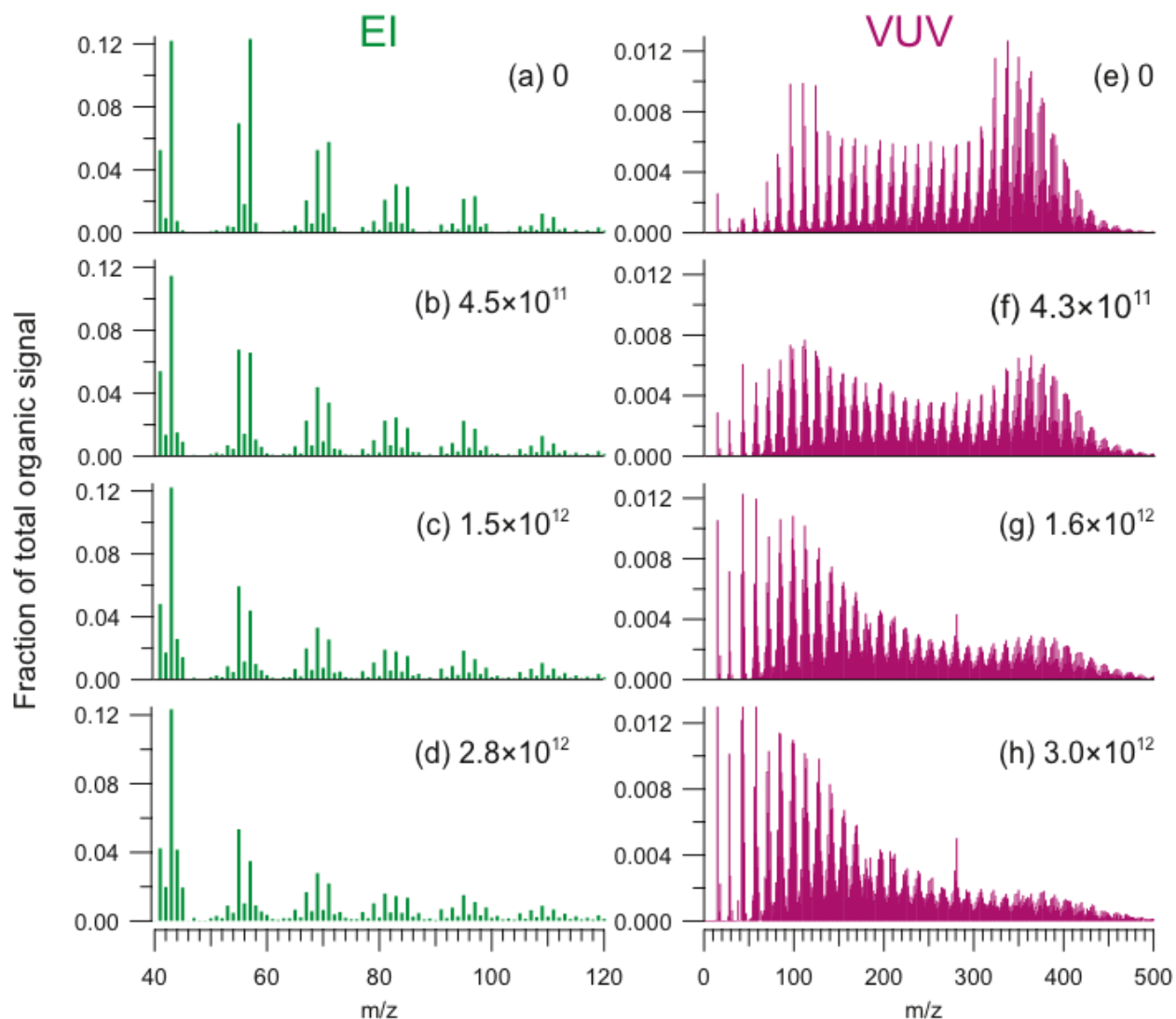


Figure 2. Mass spectra (shown in unit-mass resolution) of diesel exhaust particles at different levels of oxidation. The top panels (a and e) correspond to unreacted diesel exhaust; lower panels correspond to particles after exposure to different OH levels (OH exposures are provided in each panel, in units of molecule $\text{cm}^{-3} \text{ s}$). Left panels (a-d): electron impact ionization (EI) mass spectra. Right panels (e-h): vacuum ultraviolet photoionization (VUV) mass spectra. The peak at m/z 281 corresponds to a siloxane impurity, as confirmed by high-resolution analysis.

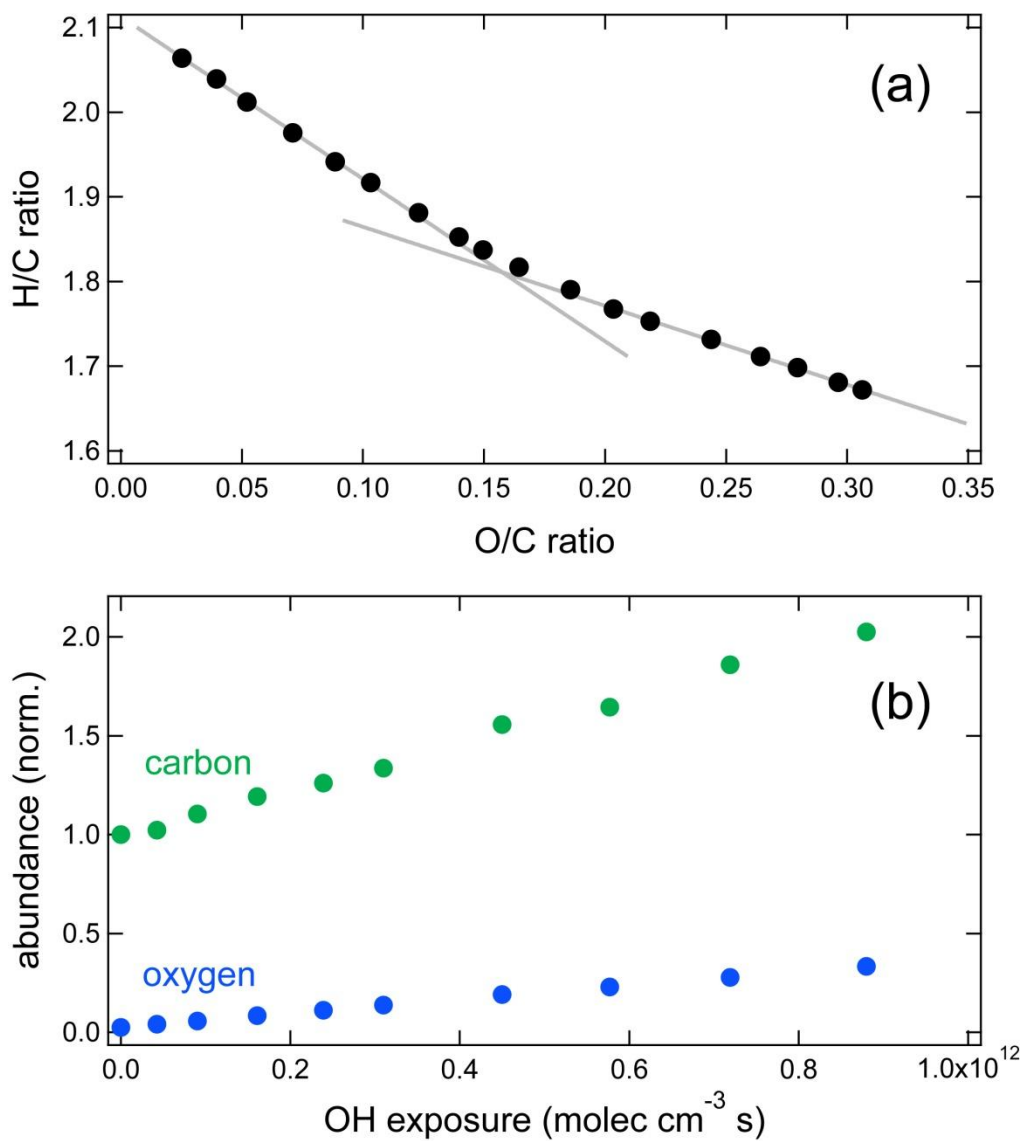


Figure 3. Evolving elemental composition of the diesel exhaust particles. Panel a: van Krevelen plot, with oxidation involving movement down and to the right. The trajectories follow two slopes, first -1.93 then -0.93. Both linear fits (determined from the six least-oxidized and the seven most-oxidized systems, respectively) are shown. Panel b: abundances of particulate carbon (green) and oxygen (blue) in the particles, normalized to the amount of carbon in the unreacted system, as a function of OH exposure [16]. The increase in carbon abundance indicates the formation of secondary organic aerosol, presumably from gas-phase semivolatile organics.

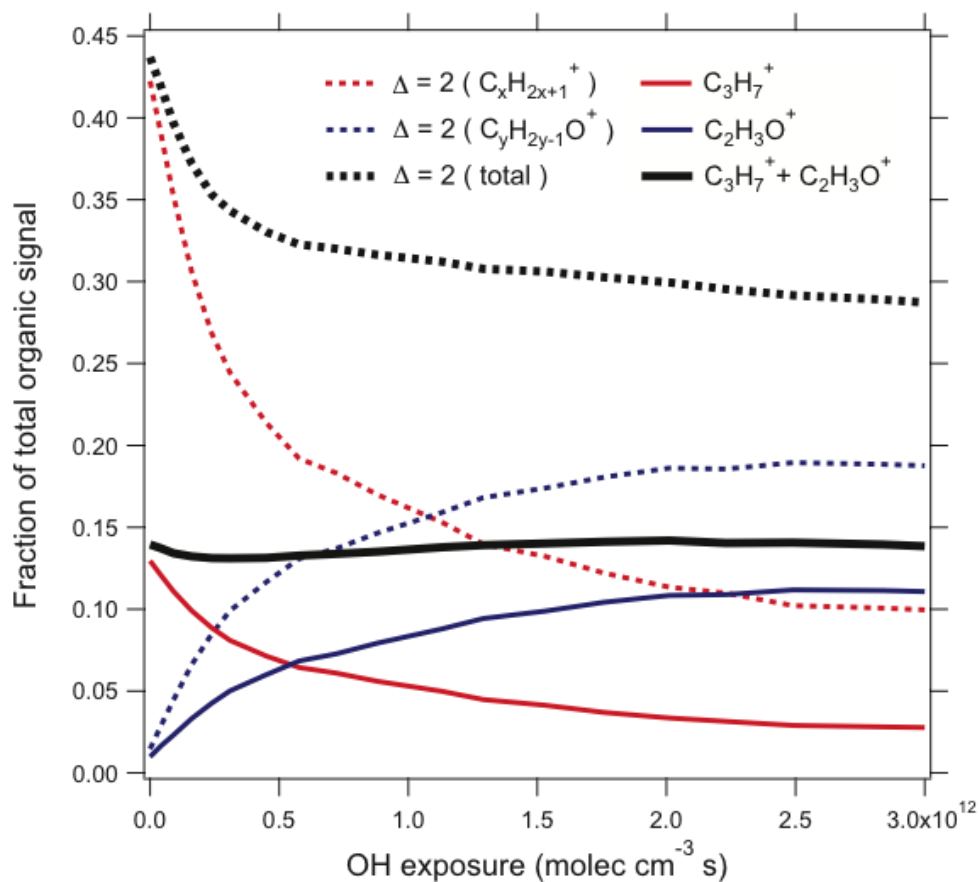


Figure 4. Normalized EI signal (ion intensity as a fraction of total) of the m/z 43 ions (solid lines) and all ions in the $\Delta=+2$ series (dotted lines). Changes to individual ions, as determined at high resolution, are much more dramatic than at a given nominal mass, due to the simultaneous decrease in $C_xH_{2x+1}^+$ ions and increase in $C_yH_{2y+1}O^+$ ions.

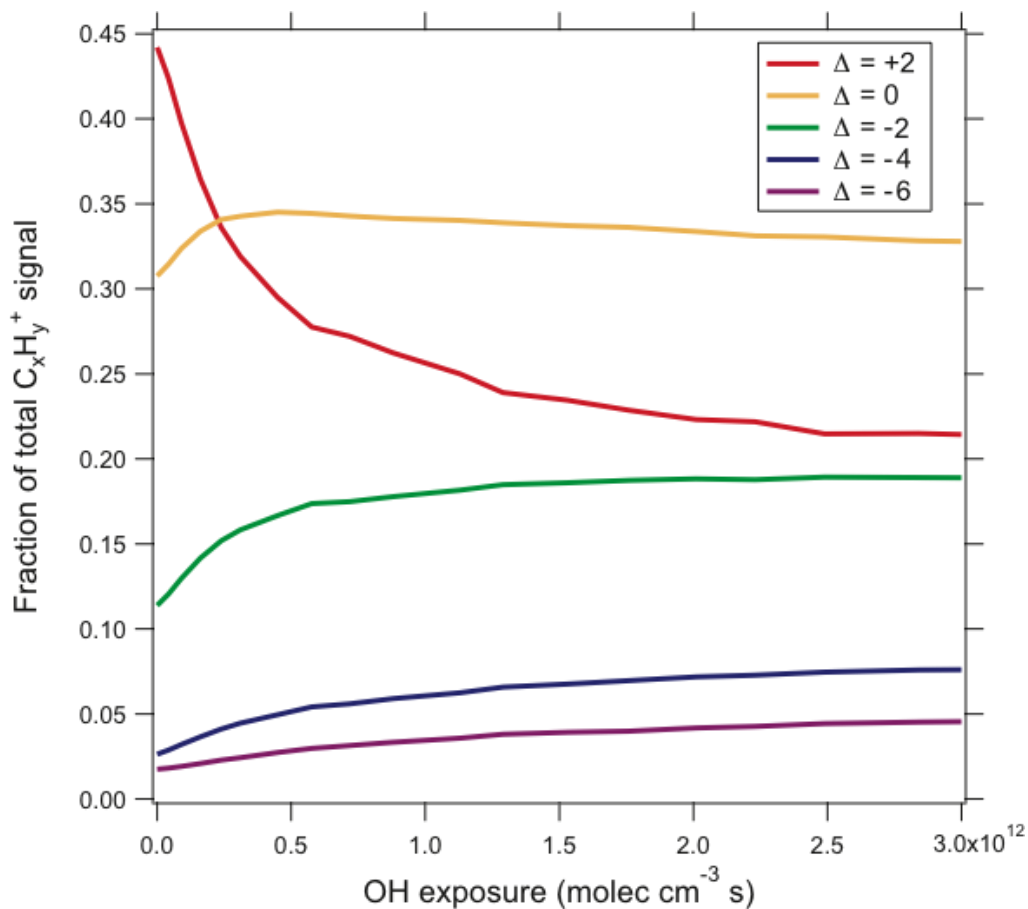


Figure 5. Evolution of the hydrocarbon ions (of form $C_xH_y^+$) in the EI mass spectra. Contributions of $C_xH_y^+$ ions in each delta series, as a fraction of the total $C_xH_y^+$ signal, are plotted against OH exposure. As oxidation increases, the $\Delta=+2$ series gives way to $\Delta=0$, as well as $\Delta=-2$, -4 , and -6 . These lower Δ -series hydrocarbon ions are likely derived from oxidized organics, which may lose oxygen during heating or ionization within the AMS.

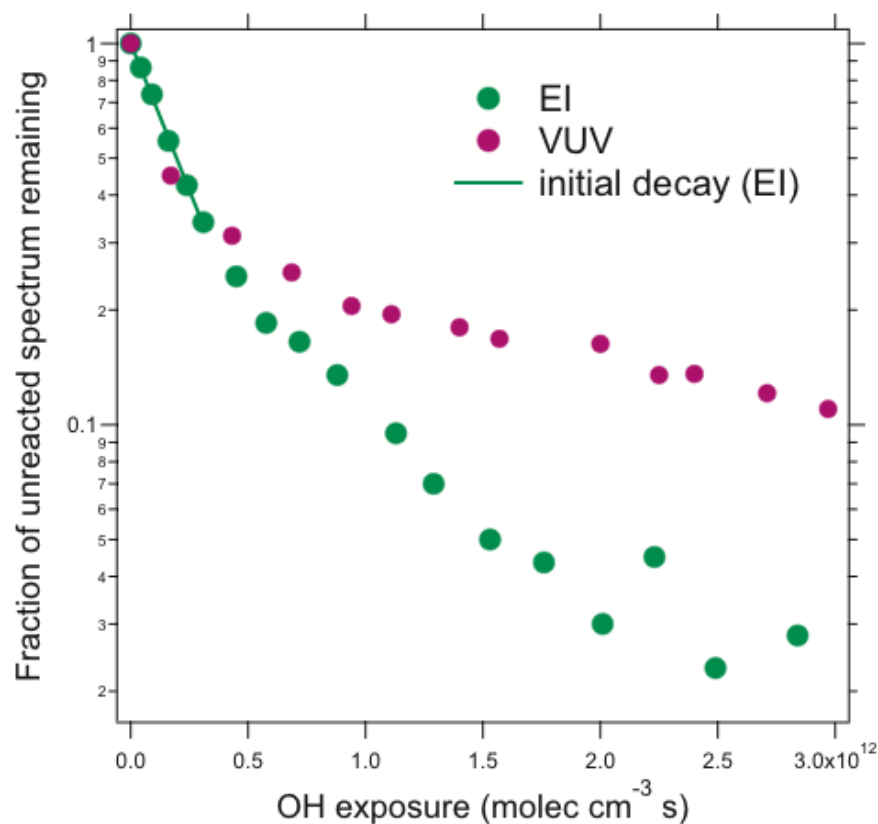


Figure 6. Reactive loss of the particulate organics in diesel exhaust. The fraction of unreacted organics remaining in the particle, as calculated by spectral subtraction (see text), is plotted versus OH exposure, for both EI and VUV data. The solid line is an exponential fit to the initial decay (EI data only), allowing for the determination of the reaction rate and effective uptake coefficient.

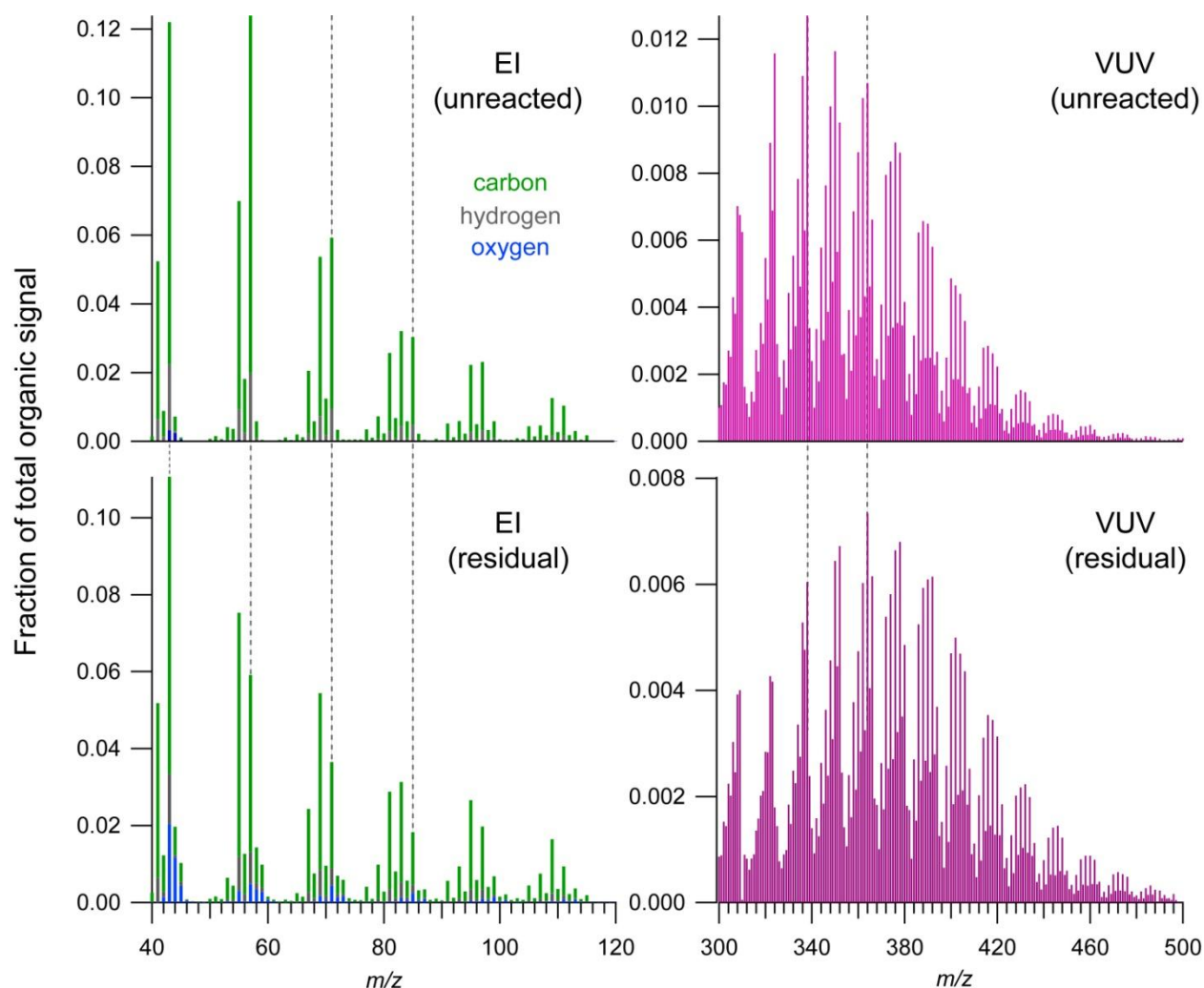


Figure 7. Reactant and product mass spectra for the initial aging of diesel exhaust particles. Top panels: unreacted diesel exhaust particles in EI and VUV (same as Fig. 2a and 2e, respectively). The EI spectra are colored by the mass contribution of different elements at each nominal m/z value. Bottom panels: EI and VUV product mass spectra, determined from spectral subtraction of the unreacted spectra from the spectra of oxidized diesel exhaust particles, at the lowest level of OH exposure studied (4.3×10^{10} molecule cm^{-3} s for EI and 1.7×10^{11} molecule cm^{-3} s for VUV). Vertical dashed lines highlight key differences in the residual spectra: major $\Delta=+2$ masses (m/z 57, 71, and 85) for EI, and the most intense molecular peaks (m/z 338 and 364) for VUV.